Case Studies in Construction Materials 18 (2023) e02183

Contents lists available at ScienceDirect

Case Studies in Construction Materials

journal homepage: www.elsevier.com/locate/cscm

Case study

Prediction of shear capacity of RC beams strengthened with FRCM composite using hybrid ANN-PSO model

Trong-Ha Nguyen, Ngoc-Long Tran, Van-Tien Phan, Duy-Duan Nguyen *

Department of Civil Engineering, Vinh University, Vinh 461010, Viet Nam

A R T I C L E I N F O

Keywords:
Artificial Neural Network (ANN)
Particle Swarm Optimization (PSO)
Reinforced concrete beam
Fiber reinforced cementitious matrix (FRCM)
Graphical user interface

A B S T R A C T

The aim of this study is to develop a hybrid Artificial Neural Network- Particle Swarm Optimization (ANN-PSO) model for improving shear strength prediction of reinforced concrete (RC) beams strengthened with fiber reinforced cementitious matrix (FRCM). A set of 89 experimental test results of strengthening RC beams are collected and used for developing the ANN-PSO model. The performance results of ANN-PSO are compared with those of pure ANN model. Typical statistical properties including the coefficient of determination (R^2), root mean squared error (*RMSE*), and the number of predicted data falling in a deviation of $\pm$ 20% compared with experimental data ($a20-index$) are calculated to evaluate the accuracy of those models. The comparisons reveal that ANN-PSO outperforms the ANN model with R^2, *RMSE*, and $a20-index$ values of 0.937, 6.02, and 0.842, respectively. Moreover, the effects of input parameters (i.e., beam geometry, concrete and reinforcement properties, and FRCM composite parameters) on the predicted shear strength are quantified. Additionally, an efficient graphical user interface (GUI) tool is developed for facilitating the practical design process of the strengthening RC beams.

1. Introduction

Reinforced concrete (RC) structures have been constructed worldwide. Overall, civil structures have been designed with a certain lifetime. Nevertheless, structural members are degraded its loading capacity after an operating period due to the influence of loadings and environmental factors. Therefore, a strengthening of corrored RC structures is required.

So far, several techniques have been employed for retrofitting RC and masonry structures using advanced materials such as textile-reinforced mortar (TRM), self-compacting concrete jacket, and fiber-reinforced polymer (FRP). Normally, textile-reinforced mortar is utilized for the shear strengthening of RC beams [5,20,51,67]. Their experiment results emphasized that the shear capacity was significantly improved, and a shear failure could be transformed to a flexure failure if using a sufficient TRM layer. In the study of Chalioris et al. [11], a series of exprimental tests were carried out to evaluate the improvement of RC beams strengthened by self-compacting concrete jacket. They showed that the load bearing capacities of retrofitted beams increased from 35% to 50%. For using FRP composite, the RC structures showed a substantial enhancement of flexural and shear strength, ductility, and durability [8,25,26,35,56,60,74]. Additionally, the FRP jackets were applied for retrofitting of corroded RC beams [4,17,68]. This retrofitted method reduces the construction time and requires a simple process. Nevertheless, there are existing drawbacks such as costly repair and debonding at the interface between FRP and concrete.

* Corresponding author.
E-mail address: duyduankxd@vinhuni.edu.vn (D.-D. Nguyen).

https://doi.org/10.1016/j.cscm.2023.e02183
Received 8 April 2023; Received in revised form 25 May 2023; Accepted 31 May 2023
Available online 1 June 2023

The steel fibers reinforce concrete/mortar (FRC/FRM) is also increasingly used in construction materials. FRC can significantly enhance the compressive and tensile strength of concrete. Additionally, it can improve the load-bearing capacity and reduce the crack development of structural members [1,46,54]. Shah & Naaman [55] concluded that the flexural strength of steel FRM was significantly increased compared to that for the plain mortar specimen. Moreover, since the construction technique is simple, FRC/FRM has been utilized for improving the structural capacities of flexural components [28].

Fiber reinforced cementitious matrix (FRCM) is a composite material, which is made up of cement-based matrix and high-strength fibers [57,61]. The fibers are typically made from materials such as steel, glass, carbon, or synthetic fibers (PBO) are added to the cement mixture to increase its strength and durability. FRCM is commonly used in building and construction applications where high strength and durability are required, such as in the reinforcement of concrete structures or the repair of damaged concrete surfaces. This kind of material was applied for strengthening masonry structures [6], beam-column joints [21]. Numerous experimental studies investigated the effects of FRCM on the flexure [18,19,58] and shear capacity [9,15,24,25,32,71] of RC beams. They highlighted that FRCM provides a significant role in increasing the flexure and shear strength of the RC beams. However, a rapidly predictive model considering a wide range of various input parameters of designed RC beams is necessary.

Recently, with the development of computing techniques, machine learning (ML) models has been applying popularly in structural engineering [29–31,44,65]. Artificial Neural Network (ANN) is one of the most preferential ML models applying for RC structures [3, 34,40,42,43,52,53,62,64,69,73,75]. Meanwhile, Particle Swarm Optimization (PSO), a computational algorithm inspired by the social behavior of bird flocks and fish schools, has been widely employed in civil and structural engineering [12,38]. Specially, PSO is normally combined with other ML algorithms for improving the prediction problems of RC structures, in which the PSO-ANN model is a typical approach [10,14,27,37,41]. Efficient ML models for shear capacity prediction of RC beams strengthened with various materials are required.

Several studies developed ML models for predicting structural capacity of RC beams retrofitted with composite materials. Wakjira et al. [72] developed ML-based models for flexural capacity prediction of RC beams strengthened with inorganic composites. Abuodeh et al. [2] used ML models to investigate the behavior of RC beams strengthened in shear with external FRP sheets. Recently, the shear strength prediction of FRP-RC beams using deep learning was conducted by Marani and Nehdi [36]. Various ML models were also developed to estimate shear capacity for steel FRC beams [13,33,50,59] and RC beam strengthen with FRP [2,7,22,36,49,70]. Even though ANN model has some advantages, however some drawbacks exist such as required large amounts of data to achieve high accuracy, susceptible to overfitting problem, interpretation issue, and significant time for training. Therefore, a combination of ANN and PSO can be a feasible option for improving the pure ANN model since ANN-PSO contains some merit such as improved accuracy, fast training, handling noisy and incomplete data, and automated feature selection. Moreover, the use of PSO-ANN for predicting the shear capacity of RC beams strengthened with FRCM composite is not well-studied yet.

This study develops a hybrid ML model, namely PSO-ANN, for improving the shear strength prediction of RC beams strengthened with the FRCM composite. For that, a total of 89 tested specimens of strengthening RC beams are collected and employed to construct the ANN-PSO model. The performance of ANN-PSO is compared with that of pure ANN model. Typical statistical properties including R^2, RMSE, and a20-index are calculated to evaluate the accuracy of those models. Moreover, the effects of input parameters on the predicted shear strength are quantified. Finally, a practical graphical user interface (GUI) tool is built for simplifying the design process of the RC beams strengthened with FRCM.

2. Data collection

To develop the ML model, a set of datasets must be collected. In this study, we gather the database based on the 89 experimental results, which were published in the literature [24]. There are 14 input parameters in the datasets including beam width (b_w), effective beam depth (d), shear span to effective depth ratio (a/d), compressive strength of concrete (f'_c), longitudinal reinforcement ratio (ρ_l), transverse reinforcement ratio (ρ_w), spacing of FRCM strips (s_f), width of FRCM strips (w_f), elastic modulus of fibers (E_f), tensile strength of fibers (f_t), number of fiber layers (n), fiber reinforcement ratio (ρ_f), cementitious matrix compressive strength (f'_{cm}), and FRCM reinforcement ratio (ρ_{cm}). Meanwhile, the shear strength contributed by FRCM (V_{FRCM}) is considered as the output variable. It should be noted that the database contains various types of fibers (i.e., carbon, glass, basalt, and synthetic fibers), beam geometry (i.e., rectangular and T-beam), strengthening configurations (i.e., side bonded, U-wrapped, and fully wrapped), and number of strengthening layers. In the database, carbon, glass, and synthetic fibers accounted for 54%, 25%, and 11%, respectively. Moreover, there are up to 79% of rectangular cross-sectional beams, and 21% remaining are for T-shaped beams. Meanwhile the number of beams

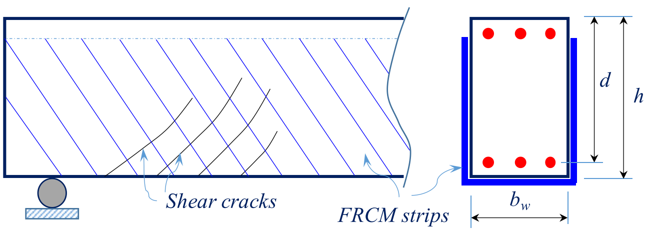

Fig. 1. Depiction of RC beams strengthening with FRCM composite.

strengthened with one FRCM layer accounted for 55%. Fig. 1 illustrates the strengthening of RC beams using FRCM composites. Table 1 summarizes the statistical parameters of the used datasets. The histogram of the datasets is shown in Fig. 2. Moreover, the correlation between the input and output variables is demonstrated in Fig. 3. Detailed information of the database is shown in the Appendix.

3. Machine learning models

3.1. Normalized training data

To improve the accurate performance of ANN and ANN-PSO models, training data is normalized within the range of − 1 and 1 prior to developing the ML models, according to the suggestion of Golafshani & Ashour [23]. The normalization is expressed in Eq. (1).

$$X_n = 2 \times \frac{(X - X_{\min})}{(X_{\max} - X_{\min})} - 1 \tag{1}$$

where X_n is the normalized sample, X is the original sample, $X_{\max}$ and $X_{\min}$ are the maximum and minimum value of each variable, respectively. The normalized values have been put into the ANN model and conducted by the MATLAB tool.

3.2. Artificial neural network algorithm

Among ML models, ANN has been commonly employed to solve various engineering problems ([39,40,42,43,47,48,63,66,75]). An ANN is a type of ML that is inspired by the structure and function of the biological neural networks in the human brain. ANNs consist of interconnected processing nodes or "neurons" that can receive, transform, and transmit information in parallel, using weighted connections and activation functions. In this study, the back propagation neural network combined with the Levenberg-Marquardt algorithm was chosen, in which a three-layers structure was adopted. The model structure includes input, hidden, and output layers. The connection between three layers is adjusted by the weights and biases of neurons. The mathematical expressions are shown as follows.

$$f : X \in R^D \rightarrow Y \in R^1$$

$$f(X) = f_0(b_2 + W_2(f_h(b_1 + W_1 X))) \tag{2}$$

where b_1, W_1, and f_h are the biases vectors, the weight matrix, and the activation function of the hidden layer, respectively. Meanwhile, b_2, W_2, and f_0 are the biases vector, the weight matric and the activation function of the hidden layer output layer, respectively.

The used activation function for the hidden layer was a nonlinear function, namely *tansig* function. And linear function, so-called *purelin* function, was selected for the output layer [45]. The equations representing the activation functions *tansig* and *purelin* are expressed in Eq. (3) and Eq. (4), respectively, and shown in Fig. 4.

$$tansig(x) = \frac{2}{(1 + \mathrm{epx}(-2x))} - 1 \tag{3}$$

$$purelin(x) = x \tag{4}$$

The training of the ANN model was performed in terms of continuous feedback loops. To obtain the optimal model during training, the mean square error (*MSE*) was employed, in which *MSE* is represented by the following expression.

Table 1
Statistical properties of input and output parameters.

Parameter		Units	Minimum	Mean	Maximum	Standard deviation (SD)	Coefficient of variation (CoV)
b_w (mm)	(X1)	mm	102.000	300.000	153.101	44.259	0.289
d (mm)	(X2)	mm	159.000	419.000	271.371	75.567	0.278
a/d	(X3)	-	2.220	4.900	2.797	0.402	0.144
$f_c^{'}$ (MPa)	(X4)	MPa	10.100	46.200	29.008	8.766	0.302
ρ_l	(X5)	-	0.008	0.051	0.025	0.012	0.486
ρ_w	(X6)	-	0.000	0.005	0.001	0.002	1.600
s_f (mm)	(X7)	mm	1.000	275.000	35.966	78.329	2.178
w_f (mm)	(X8)	mm	1.000	200.000	19.247	43.784	2.275
E_f (GPa)	(X9)	GPa	31.900	270.000	178.227	85.389	0.479
f_t (MPa)	(X10)	MPa	574.000	5800.000	3046.854	1662.851	0.546
n	(X11)	-	1.000	6.000	1.764	1.118	0.634
ρ_f	(X12)	-	0.000	0.006	0.001	0.001	0.909
$f_{cm}^{'}$	(X13)	MPa	21.800	86.700	44.206	19.457	0.440
ρ_{cm}	(X14)	-	0.017	0.240	0.107	0.060	0.564
V_{FRCM}	(Output)	kN	2.700	87.500	35.282	21.462	0.608

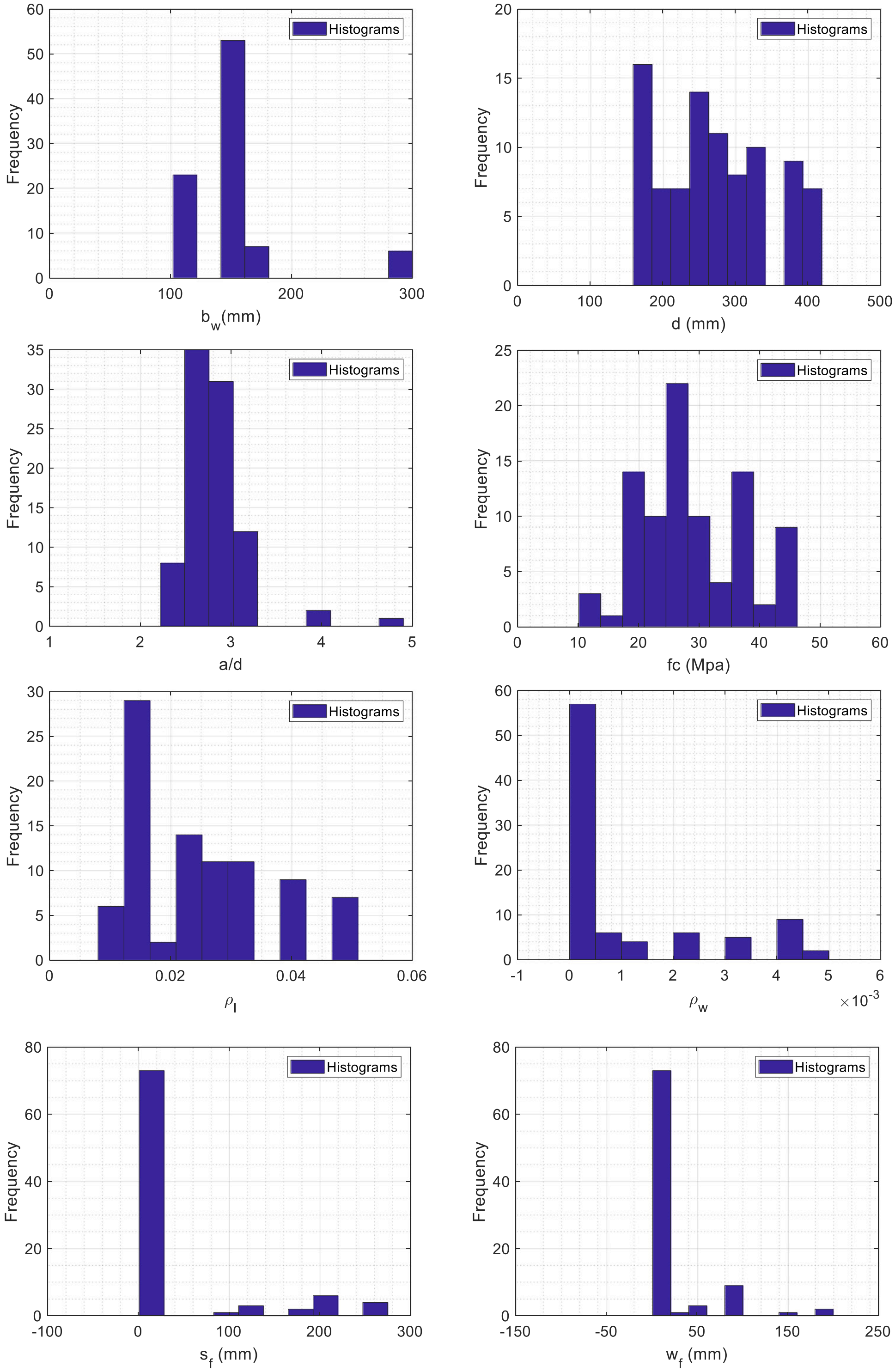

Fig. 2. Histograms of the dataset.

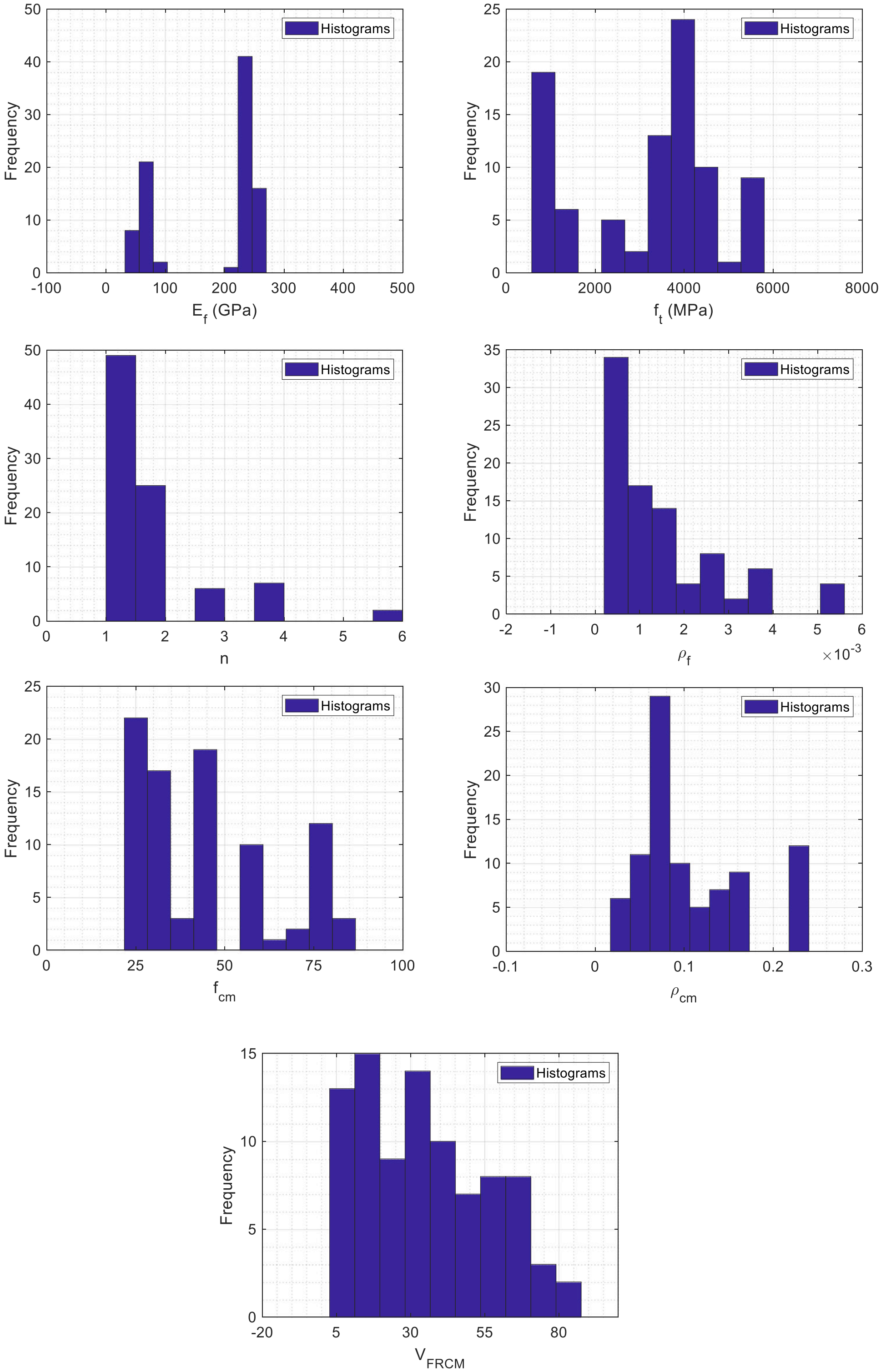

Fig. 2. (*continued*).

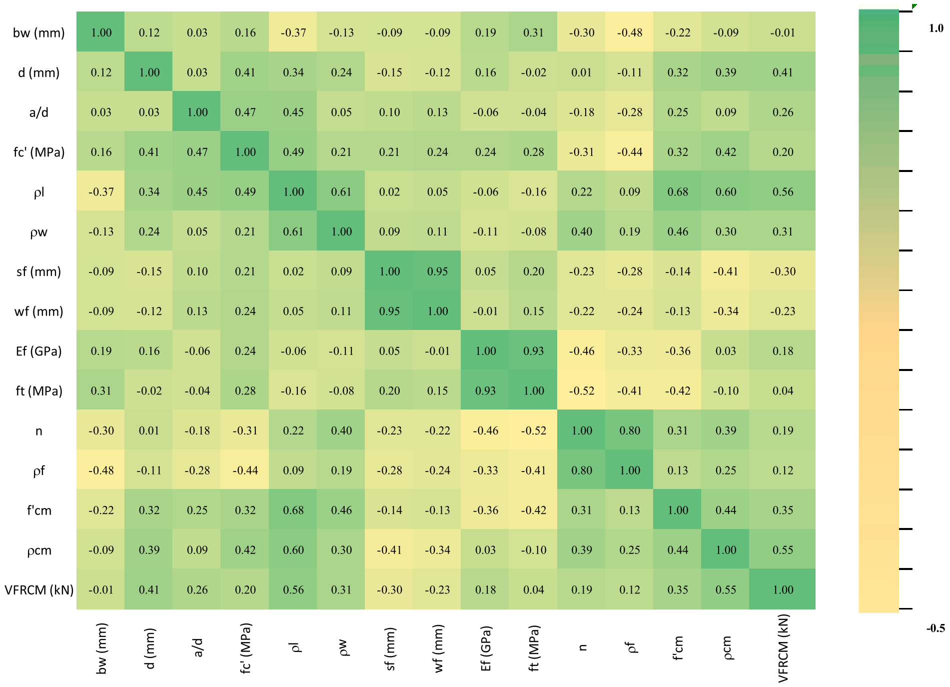

Fig. 3. Correlation matrix between the input and output parameters.

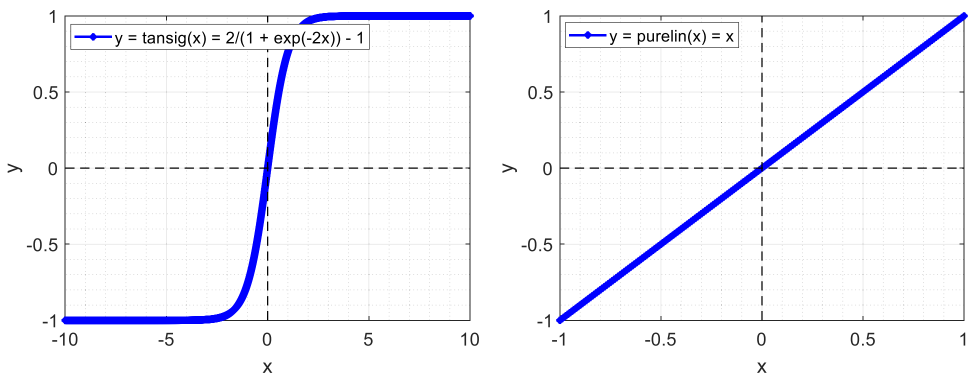

Fig. 4. Activation functions: *tansig* and *purelin*.

$$MSE = \min_{b_1, b_2, W_1, W_2} \frac{1}{N} \sum_{i=1}^{N} e_i^2 \tag{5}$$

where e_i is the difference between the predicted output and the experimental data; N is number of samples of the ANN model.

3.3. Artificial neural network-Particle swarm optimization (ANN-PSO) model

PSO is a computational algorithm inspired by the social behavior of bird flocks and fish schools, was first introduced by Eberhart and Kenedy [16]. PSO works by creating a group of particles, where each particle represents a potential solution to an optimization problem. The particles move through the search space, adjusting their position based on their own experience and the experience of their neighbors. By doing so, the particles converge towards the optimal solution of the problem. PSO is commonly used in optimization problems that involve many variables and is known for its simplicity and efficiency.

The optimization procedure is based on the positions and velocities of all particles corresponding to the states of the system. Let x_l^i denotes the position vector of the particle i at l-the generation, v_l^i represents the velocity vector, y^i indicates the best position explored by individual particle, and $\hat{y}$ depicts the global best. The velocity and position vectors of each particle are updated by the following expressions.

$$v_{l+1}^{i} = w_l v_l^{i} + c_1 R_1 \left(y^{i} - x_l^{i}\right) + c_2 R_2 \left(\widehat{y} - x_l^{i}\right) \tag{6}$$

$$x_{l+1}^{i} = x_l^{i} + v_{l+1}^{i} \tag{7}$$

where w_l is the inertia weight; c_1 and c_2 are the acceleration coefficients; R_1 and $R_1 \in [0,1]$ are the uniform and independent random numbers.

The ANN-PSO model is a machine learning technique that combines two powerful algorithms, ANN and PSO. It is used to train neural networks for solving complex problems, such as image recognition, speech recognition, and natural language processing. In this model, the neural network is first created and initialized with random weights. Then, the PSO algorithm is applied to find the optimal set of weights for the neural network. The PSO algorithm works by simulating the behavior of a swarm of particles, which move through a multidimensional search space and look for the optimal solution. By combining these two algorithms, the ANN-PSO model can effectively optimize the weights of the neural network, resulting in better accuracy and faster convergence times. The flowchart of the hybrid PSO-ANN model is shown in Fig. 5.

3.4. Statistical indicators for ML model evaluation

An ANN model achieves the best performance at the split ratio (training, testing, and validation) combined with the number of hidden layers and neurons in the hidden layer. To evaluate the optimal model, three statistical indicators, which include coefficient of determination (R^2), root mean squared error ($RMSE$), and $a20-index$ were employed to measure the accuracy of the predictive models, as suggested by Zorlu et al. [75]. They are expressed as follows.

$$R^2 = 1 - \left(\frac{\sum_{i=1}^{N}(t_i - o_i)^2}{\sum_{i=1}^{N}(t_i - \overline{o})^2}\right) \tag{8}$$

$$RMSE = \sqrt{\left(\frac{1}{n}\right)\sum_{i=1}^{n}(t_i - o_i)^2}; \tag{9}$$

$$a20 - index = \frac{n20}{n} \tag{10}$$

where t_i and o_i represent the target and output of i^{th} data point, respectively; $\overline{o}$ is the mean of output data samples; n is the number of samples; $n20$ is the number of samples with the ratio of the experimental value to the predicted value between 0.8 and 1.0.

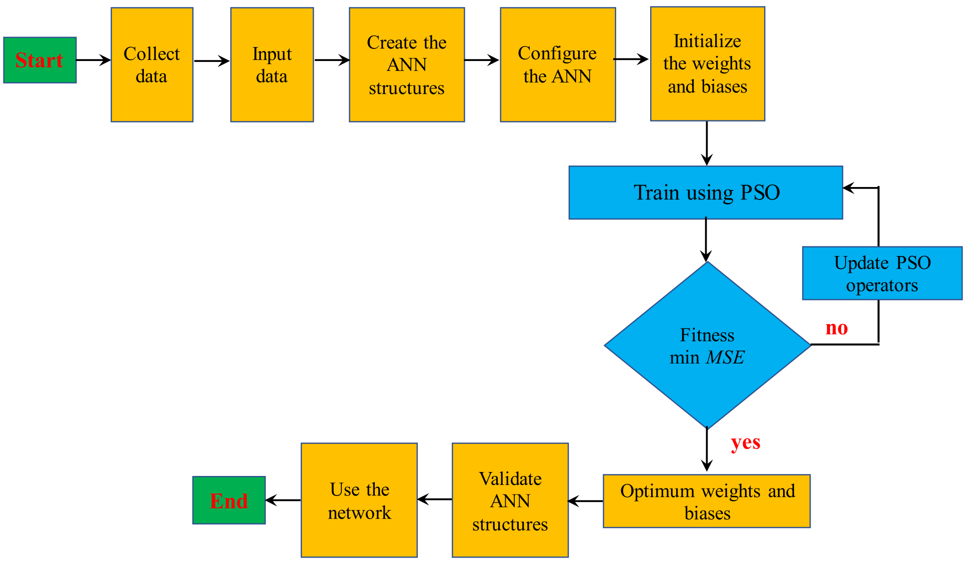

Fig. 5. Flowchart of the ANN-PSO model.

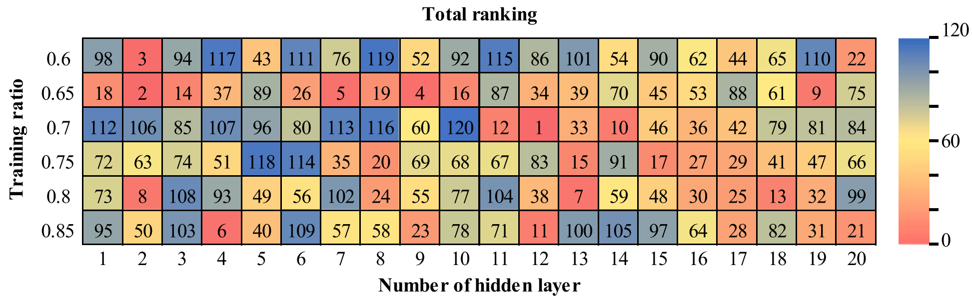

Fig. 6. Ranking of various ANN structures.

4. Results and discussions

4.1. Performance results of ANN model

To obtain the optimum ANN model, a total of 120 ANN structures were tested, in which various data training ratios were changed, i.e., 0.6, 0.65, 0.7, 0.75, 0.8 and 0.85. Meanwhile, the data testing and validation ratios were taken a haft of the remaining. Additionally, the number of neurons in the hidden layer varied from 1 to 20. The tested models were evaluated using three statistical indicators

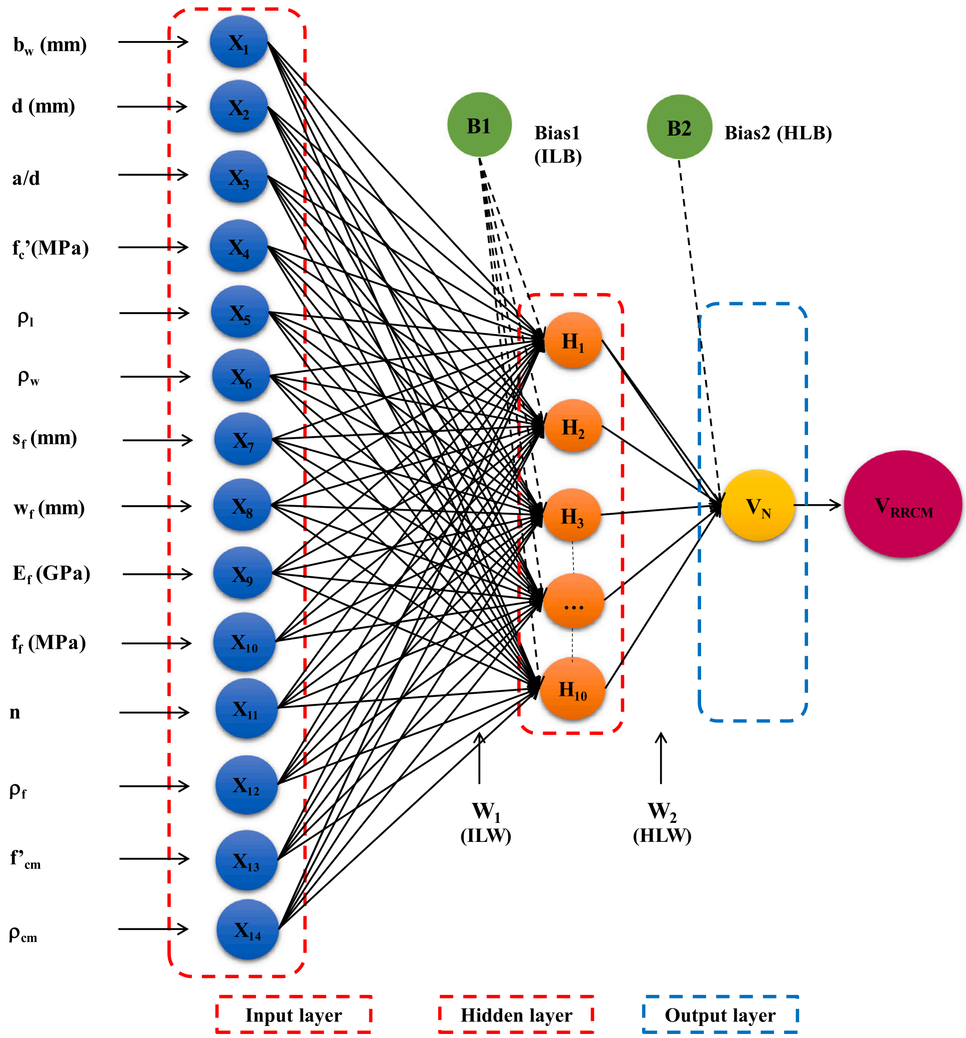

Fig. 7. Proposed structure of ANN.

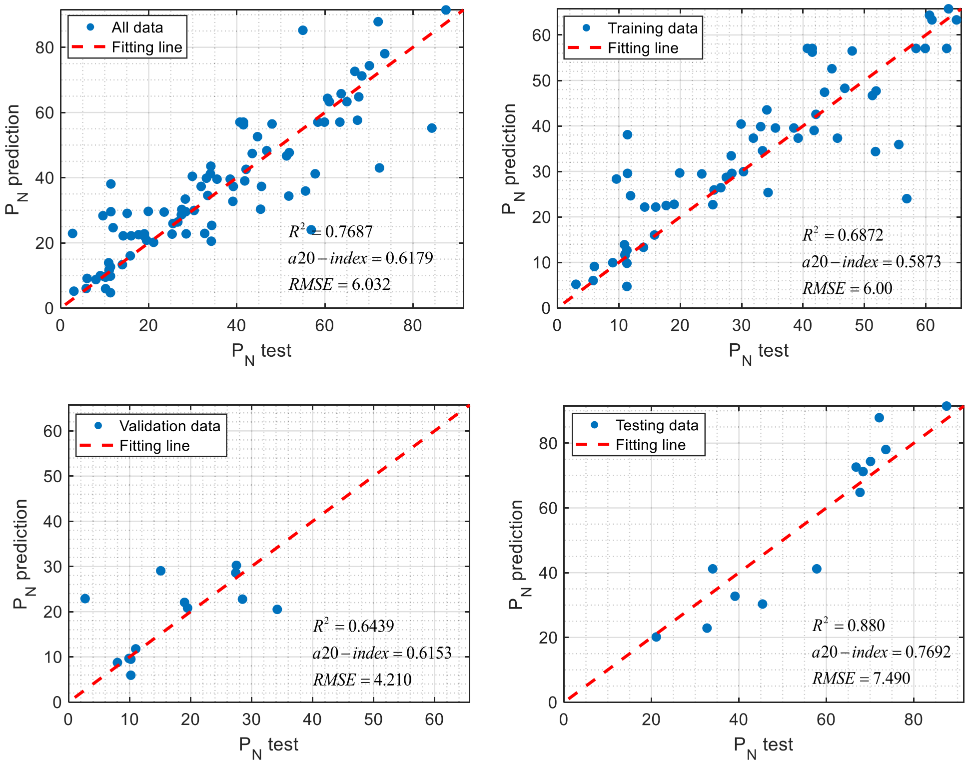

Fig. 8. Regression performance of ANN model.

Table 2
Statistical properties of ANN performance.

	R^2	*RMSE* (kN)	*a20-index*	$V_{FRCM}^{test}/V_{FRCM}^{predict}$				
				Min	Mean	Max	SD	CoV
All data	0.7687	6.032	0.6179	0.1180	0.9920	2.4012	0.3568	0.3596
Training	0.6872	6.000	0.5873	0.2994	0.9747	2.4012	0.3673	0.3768
Validation	0.6439	4.210	0.6153	0.1180	0.9920	1.7195	0.4169	0.4203
Testing	0.8800	7.490	0.7692	0.8207	1.0758	1.4973	0.2310	0.2147

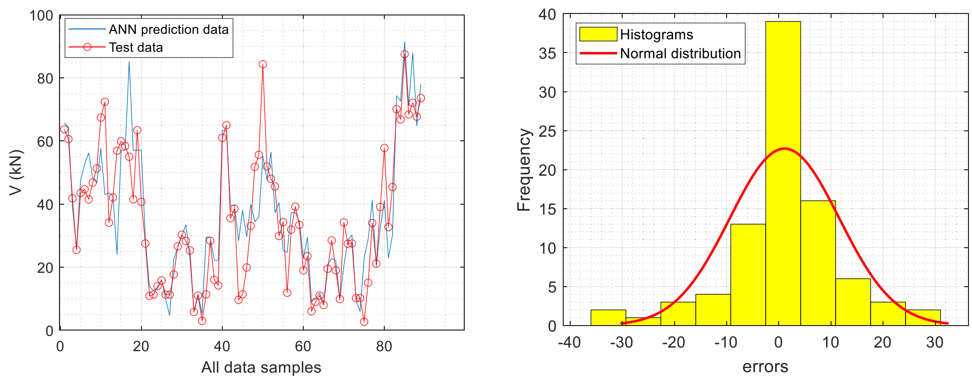

Fig. 9. Errors between predicted ANN model and experiments.

including R^2, $RMSE$, and $a20 - index$, as ranked in Fig. 6. As a result, the optimal model was selected based on the highest R^2, and smallest values of $RMSE$, and $a20 - index$. The used ANN model contained the data training, testing, and validation ratios were 0.7, 0.15, 0.15, respectively, and 10 neurons in the hidden layer, as shown in Fig. 7. It should be noted that the optimal ANN structure in Fig. 7 will be used for development of the hybrid PSO-ANN model.

Training results of the ANN model are shown in Fig. 8 and Table 2. It can be found that R^2 values obtained for training, testing, validation, and all data were 0.6872, 0.880, 0.6439, and 0.7687, less than 0.8. Additionally, the $a20 - indices$ were approximately 60%. Moreover, the standard deviation of the ratio $V_{FRCM}^{test}/V_{FRCM}^{predict}$ was larger than 0.35. The errors between predicted ANN model and experiment are shown in Fig. 9. Those results imply that the ANN model was less reliable for predicting the shear strength of RC beams strengthened with FRCM. Therefore, it is necessary to improve the predictive ANN model by an optimization technique.

4.2. Performance results of ANN-PSO model

The convergence of PSO-ANN model was obtained after 1000 iterations and the mean square error (MSE) was very small (almost zero). Moreover, performance results of the PSO-ANN model are shown in Fig. 10 and Table 3. It can be observed that R^2 values obtained for training, testing, validation, and all data were 0.917, 0.960, 0.937, and 0.937. Besides, the $a20 - indices$ were larger than 80%. The standard deviation of the ratio $V_{FRCM}^{test}/V_{FRCM}^{predict}$ was smaller than 0.2. The errors between predicted PSO-ANN model and experiment are shown in Fig. 11. Those performance results indicate that the hybrid PSO-ANN model significantly improved the shear strength prediction of RC beams strengthened with FRCM.

A comparison of performance results between ANN and PSO-ANN is shown in Fig. 12. It can be found that the PSO-ANN outperformed ANN model in terms of R^2, $RMSE$, and $a20 - index$ indicators. Specifically, R^2 values of the training set were increased from 0.69 up to 0.92, from 0.88 to 0.96 for testing set, and from 0.64 to 0.94 for validation set. Additionally, $a20 - index$ was increased from 0.59 to 0.79 for training set, from 0.77 to 1.0 for testing set, and from 0.61 to 0.92 for validation set. The SD and CoV of the ratio $V_{FRCM}^{test}/V_{FRCM}^{predict}$ for PSO-ANN were quite smaller compared to those of ANN model. Once again, it can be highlighted that PSO-ANN model is capable of shear strength prediction of RC beams strengthened with FRCM composite.

4.3. Effects of input parameters on the output

To evaluate the influence of input parameters on the shear capacity of strengthened RC beams, a series of sensitivity analyses were performed. In this study, we used Shapley value to identify the effects of input features on the output. Shapely value is a concept in cooperative game theory that provides a way to fairly distribute the worth or value among the players in a game. The Shapely value

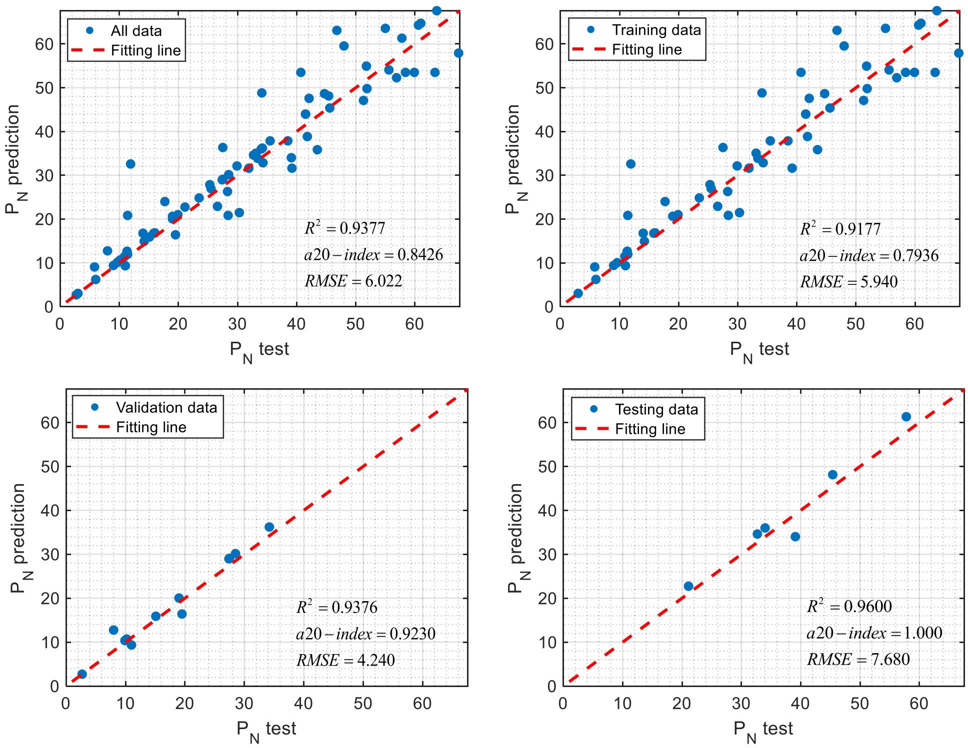

Fig. 10. Performance of the ANN-PSO model.

Table 3
Statistical properties of PSO-ANN performance.

Data sets	R^2	*RMSE* (kN)	*a20-index*	$V^{test}_{FRCM}/V^{predict}_{FRCM}$ Min	Mean	Max	S	CoV
All data	0.9377	6.022	0.8426	0.3653	0.9698	1.4900	0.1634	0.1685
Training	0.9177	5.940	0.7936	0.3653	0.9719	1.4900	0.1830	0.1883
Validation	0.9376	4.240	0.9230	0.6278	0.9646	1.1890	0.1330	0.1379
Testing	0.9600	7.680	1.0000	0.8637	0.9651	1.1496	0.0709	0.0735

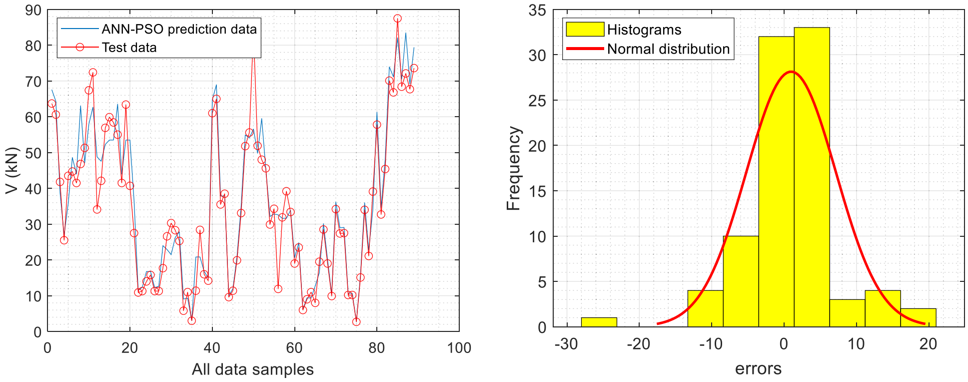

Fig. 11. Error between ANN-PSO and experimental results.

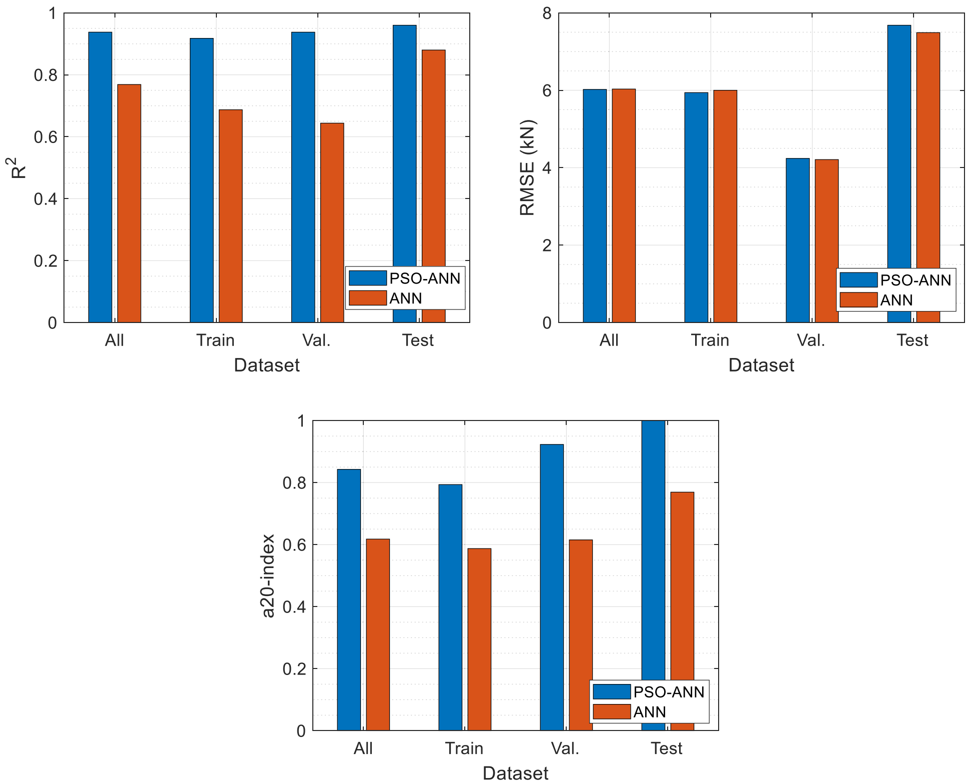

Fig. 12. Comparison between the results of ANN and PSO-ANN models.

considers all possible coalitions of players and assigns a share of the total value generated by each coalition to each player. In machine learning, the Shapely value can be used to explain the predictions of a model by attributing a value to each feature or input variable in a dataset. This can be useful for understanding which features are the most important and how they contribute to the output of the model. By using the Shapely value, any interactions or dependencies that may exist between the features can be also identified.

To calculate the Shapely value, the following basic steps can be followed:

- Define the characteristic function: This function maps any coalition of variables to a value that represents the worth of that coalition.
- Calculate the marginal contribution of each variable to each coalition: Marginal contribution is the difference between the worth of a coalition with and without a variable.
- Calculate the average marginal contribution of each variable across all possible coalitions in which they participate: This is done by taking the sum of the marginal contributions for each coalition in which the variable participates and dividing by the total number of such coalitions.
- Sum the average marginal contributions over all possible subsets of variables: This gives the Shapely value for each input variable.

The Shapley value result for each variable is shown in Fig. 13. It can be found that the elastic modulus of fibers (E_f) showed to be the most influential parameter on the shear capacity of RC beams strengthen with FRCM, followed by tensile strength of fibers (f_t), longitudinal reinforcement ratio (ρ_l), transverse reinforcement ratio (ρ_w), and width of FRCM strips (w_f). Meanwhile, the spacing of FRCM strips (s_f) and compressive strength of concrete ($f_c^{'}$) negatively affected the output result.

4.4. Practical GUI tool

To simplify the design process, a practical tool should be developed for rapidly calculating the shear strength of RC beams strengthened with FRCM. In this study, we constructed a graphical user interface (GUI) tool, in which designers only need to provide 14 input values, then they can immediately obtain the output (i.e., the shear strength) after one click. Fig. 14 shows the developed GUI tool using MATLAB. This GUI is freely to access, and it is available at https://github.com/duyduan1304/GUI_RCbeams_FRCMstrengthening.

5. Conclusions

This study develops a hybrid PSO-ANN model for predicting the shear strength of RC beams strengthened with the FRCM composite. A set of 89 tested specimens of strengthening RC beams is collected and employed to construct the ANN-PSO model. The performance results of ANN-PSO are compared with those of pure ANN model. Statistical parameters including R^2, RMSE, and a20-index are calculated to evaluate the accuracy of those models. Moreover, the effects of input parameters on the predicted shear strength are quantified. Finally, a practical graphical user interface (GUI) tool is built for simplifying the design process of the RC beams strengthened with FRCM. The following conclusions are obtained.

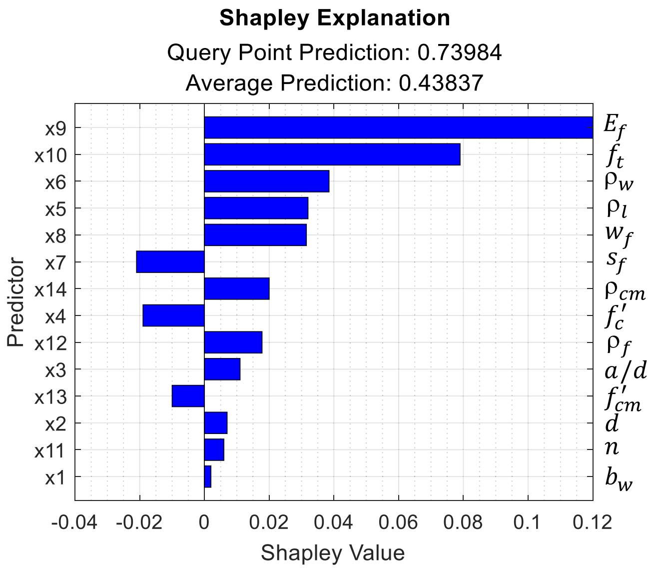

Fig. 13. Effects of input parameters on the output using Shapley value.

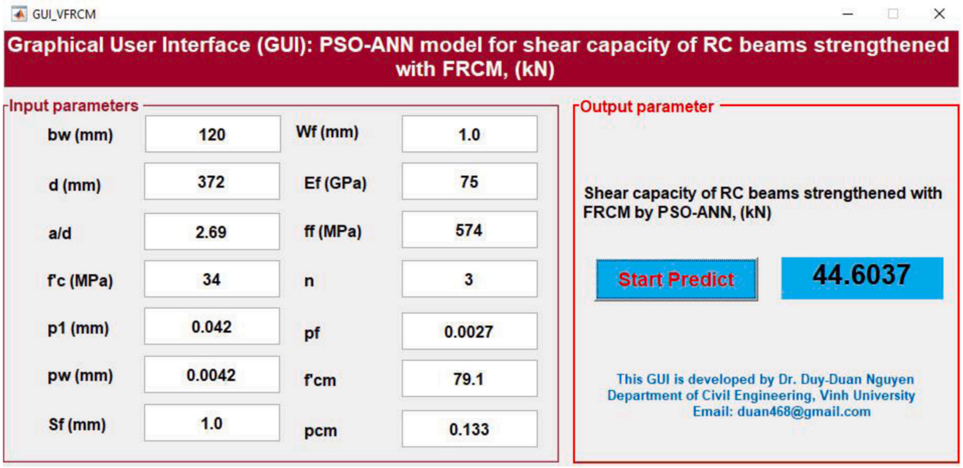

Fig. 14. Practical GUI tool.

- The PSO-ANN model can accurately predict the shear strength of RC beams strengthened with FRCM composite.
- The elastic modulus of fibers (E_f) shows to be the most influential parameter on the shear capacity of RC beams strengthen with FRCM, followed by tensile strength of fibers (f_t), longitudinal reinforcement ratio (ρ_l), transverse reinforcement ratio (ρ_w), and width of FRCM strips (w_f).
- Meanwhile, the spacing of FRCM strips (s_f) and compressive strength of concrete ($f_c^{'}$) negatively affect the output result.
- An efficient GUI tool is developed to simplify the design process of RC beams strengthened with FRCM.

Even though the ANN-PSO developed in the current study shows an acceptable performance, the accuracy of the prediction needs to be improved with a larger number of used datasets. Moreover, more advanced ML models should be investigated to identify the optimal algorithm.

Funding statement

No funding was used in this study.

CRediT authorship contribution statement

Trong-Ha Nguyen: Conceptualization, Software, Writing – original draft, Writing – review & editing. **Ngoc-Long Tran**: Validation, Visualization. **Van-Tien Phan**: Validation, Visualization. **Duy-Duan Nguyen**: Methodology, Formal analysis, Writing – original draft, Writing – review & editing, Supervision.

Declaration of Competing Interest

The authors declare that they have no known competing financial interests or personal relationships that could have appeared to influence the work reported in this paper.

Data Availability

Data will be made available on request. The data used to support the findings of this study are included in the article.

Appendix. Detailed information of the database

ID	Geometry			Concrete	Reinforcement		FRCM composite								Output
	b_w (mm)	d (mm)	a/d	$f_c^{'}$ (MPa)	ρ_l	ρ_w	s_f (mm)	w_f (mm)	E_f (GPa)	f_t (MPa)	n	ρf	$f_{cm}^{'}$	ρcm	V_{FRCM} (kN)
1	150	272	2.85	25.3	0.015	0.0014	1	1	225	3350	2	0.0013	30.6	0.07	63.7
2	150	272	2.85	25.3	0.015	0.0014	1	1	225	3350	2	0.0012	30.6	0.07	60.6
3	150	272	2.85	25.3	0.015	0.0014	1	1	225	3350	1	0.0006	30.6	0.047	41.8

(continued on next page)

(*continued*)

ID	Geometry			Concrete	Reinforcement		FRCM composite								Output
	b_w (mm)	d (mm)	a/d	f_c' (MPa)	ρ_l	ρ_w	s_f (mm)	w_f (mm)	E_f (GPa)	f_t (MPa)	n	ρf	f_{cm}'	ρcm	V_{FRCM} (kN)
4	150	256	3.91	23.2	0.032	0	1	1	75	574	2	0.0015	77.2	0.08	25.5
5	150	256	3.91	23.2	0.032	0	1	1	75	574	3	0.0022	77.2	0.053	43.5
6	120	372	2.69	25.5	0.042	0.0042	1	1	75	574	2	0.0018	82.8	0.1	44.7
7	120	372	2.69	26.3	0.042	0.0042	1	1	75	574	4	0.0037	85.3	0.167	41.5
8	120	372	2.69	28.6	0.042	0.0042	1	1	75	574	6	0.0055	79.3	0.233	46.8
9	120	372	2.69	27.1	0.042	0.0042	1	1	75	574	2	0.0018	70.6	0.1	51.3
10	120	372	2.69	25.6	0.042	0.0042	1	1	75	574	4	0.0037	86.7	0.167	67.4
11	120	372	2.69	28.7	0.042	0.0042	1	1	75	574	6	0.0055	75.4	0.233	72.4
12	120	372	2.69	28	0.042	0.0042	1	1	75	574	3	0.0027	72	0.133	34.1
13	120	372	2.69	34	0.042	0.0042	1	1	75	574	3	0.0027	79.1	0.133	42.1
14	120	372	2.69	32	0.042	0.0042	1	1	75	574	4	0.0037	63.3	0.167	56.9
15	180	419	2.98	46.2	0.032	0	1	1	253	3800	1	0.0002	45	0.222	59.9
16	180	419	2.98	46.2	0.032	0	1	1	253	3800	1	0.0002	45	0.222	58.4
17	180	419	2.98	46.2	0.032	0	1	1	201	3800	1	0.0002	77	0.222	55
18	180	419	2.98	46.2	0.032	0	1	1	253	3800	1	0.0002	45	0.222	41.5
19	180	419	2.98	46.2	0.032	0	1	1	253	3800	1	0.0002	45	0.222	63.4
20	180	419	2.98	46.2	0.032	0	1	1	253	3800	1	0.0002	45	0.222	40.7
21	180	419	2.98	46.2	0.032	0	1	1	262	2950	1	0.0002	22	0.222	27.5
22	150	159	2.52	20	0.013	0	1	1	31.9	623	2	0.0017	23.9	0.08	10.9
23	150	159	2.52	20	0.013	0	1	1	31.9	623	2	0.0012	23.9	0.08	11.3
24	150	159	2.52	20	0.013	0	1	1	31.9	623	4	0.0034	23.9	0.133	14
25	150	159	2.52	20	0.013	0	1	1	31.9	623	4	0.0024	23.9	0.133	15.8
26	150	159	2.52	20	0.013	0	1	1	31.9	623	2	0.0017	56.4	0.08	11.3
27	150	159	2.52	20	0.013	0	1	1	31.9	623	2	0.0012	56.4	0.08	11.3
28	150	159	2.52	20	0.013	0	1	1	31.9	623	4	0.0034	56.4	0.133	17.7
29	150	159	2.52	20	0.013	0	1	1	31.9	623	4	0.0024	56.4	0.133	26.6
30	120	204	3.18	25.6	0.026	0	1	1	74	1102	1	0.0012	42	0.083	30.3
31	120	204	3.18	25.6	0.026	0	120	100	74	1102	1	0.001	42	0.139	28.3
32	120	204	3.18	25.6	0.026	0	120	100	74	1102	1	0.001	42	0.069	25.3
33	120	204	3.18	25.6	0.026	0	200	40	74	1102	1	0.0002	42	0.017	5.8
34	120	204	3.18	35.2	0.026	0	200	100	74	1102	1	0.0006	42	0.042	11
35	120	204	3.18	35.2	0.026	0	1	1	74	1102	1	0.0012	42	0.033	3
36	150	308	3.25	37.5	0.021	0	1	1	75	2300	1	0.0006	58	0.093	11.4
37	150	308	3.25	37.5	0.021	0	1	1	75	2300	1	0.0006	58	0.093	28.4
38	150	308	3.25	37.5	0.021	0	1	1	230	3800	1	0.0005	58	0.093	16
39	150	308	3.25	37.5	0.021	0	1	1	230	3800	1	0.0005	58	0.093	14.2
40	150	308	3.25	37.5	0.021	0	1	1	230	3800	1	0.0012	58	0.093	61
41	150	308	3.25	37.5	0.021	0	1	1	230	3800	1	0.0012	58	0.093	65
42	150	310	2.9	41.6	0.03	0.0021	275	200	75	2300	1	0.001	40	0.058	35.5
43	150	310	2.9	41.6	0.03	0.0021	275	200	75	2300	1	0.001	40	0.058	38.5
44	150	320	2.5	16.7	0.016	0	1	1	225	3375	1	0.0006	21.8	0.053	9.6
45	150	320	2.5	18	0.016	0	1	1	225	3375	2	0.0013	21.8	0.08	11.4
46	150	320	2.5	19.4	0.016	0	1	1	225	3375	1	0.0013	21.8	0.053	19.9
47	150	320	2.5	19.2	0.016	0	1	1	225	3375	2	0.0026	21.8	0.08	33.1
48	150	320	2.5	20.1	0.016	0	1	1	225	3375	2	0.0013	21.8	0.08	51.8
49	150	320	2.5	19.2	0.016	0	1	1	225	3375	2	0.0013	21.8	0.08	55.6
50	150	320	2.5	10.1	0.016	0	1	1	225	3375	2	0.0013	21.8	0.08	84.3
51	150	320	2.5	10.7	0.016	0	1	1	225	3375	1	0.0013	21.8	0.053	51.9
52	150	320	2.5	11.1	0.016	0	1	1	225	3375	2	0.0026	21.8	0.08	48
53	150	320	2.5	20.8	0.016	0	1	1	225	3375	2	0.0026	21.8	0.08	45.6
54	300	254	2.76	28	0.008	0.0007	1	1	95	2990	1	0.0004	24.6	0.067	29.9
55	300	254	2.76	28	0.008	0.0007	1	1	240	4320	1	0.0003	25	0.067	34.3
56	300	254	2.76	28.3	0.008	0.0007	1	1	240	4320	1	0.0003	25	0.067	11.9
57	300	254	2.76	28.3	0.008	0.0007	1	1	270	5800	1	0.0003	30	0.067	31.9
58	300	254	2.76	28.3	0.008	0.0007	1	1	270	5800	1	0.0003	30	0.067	39.2
59	300	254	2.76	28.3	0.008	0.0007	1	1	90	2610	1	0.0003	35.4	0.067	33.4
60	150	270	2.22	28	0.015	0	1	1	240	4300	1	0.0014	45	0.067	19
61	150	270	2.22	28	0.015	0	1	1	240	4300	2	0.0029	45	0.1	23.5
62	150	270	2.22	28	0.015	0	183	50	240	4300	1	0.0004	45	0.018	6
63	150	270	2.22	28	0.015	0	138	50	240	4300	1	0.0005	45	0.024	9
64	150	270	2.22	28	0.015	0	110	50	240	4300	1	0.0006	45	0.03	11
65	150	270	2.22	28	0.015	0	250	100	240	4300	1	0.0006	45	0.027	8
66	150	270	2.22	28	0.015	0	167	100	240	4300	1	0.0009	45	0.04	19.5
67	150	270	2.22	28	0.015	0	1	1	240	4300	1	0.0014	45	0.067	28.5
68	150	225	3	30.8	0.019	0.0023	1	1	270	5800	1	0.0006	30.4	0.107	19
69	150	225	3	30.8	0.019	0.0023	260	150	270	5800	1	0.0004	30.4	0.062	9.9
70	150	225	2.78	45	0.028	0.0032	1	1	270	5800	1	0.0006	30.4	0.107	34.2

(*continued on next page*)

(*continued*)

ID	Geometry			Concrete	Reinforcement		FRCM composite								Output
	b_w (mm)	d (mm)	a/d	$f_c^{'}$ (MPa)	ρ_l	ρ_w	s_f (mm)	w_f (mm)	E_f (GPa)	f_t (MPa)	n	ρf	$f_{cm}^{'}$	ρcm	V_{FRCM} (kN)
71	150	225	2.78	29.2	0.028	0.0032	1	1	270	5800	2	0.0012	30.4	0.16	27.4
72	150	225	2.78	29.2	0.028	0.0032	210	100	270	5800	2	0.0006	30.4	0.076	27.5
73	150	225	2.78	38.3	0.028	0.0032	210	100	270	5800	1	0.0003	30.4	0.051	10.2
74	150	225	2.78	38.3	0.028	0.0032	210	100	270	5800	3	0.0009	30.4	0.102	10.2
75	102	177	2.6	21.6	0.022	0	1	1	225	3800	1	0.0019	31.1	0.078	2.7
76	102	177	2.6	22.6	0.022	0	1	1	225	3800	2	0.0037	28.2	0.118	15.1
77	102	177	2.6	22.6	0.022	0	1	1	225	3800	3	0.0056	26.9	0.157	34
78	102	177	2.6	23.8	0.022	0	1	1	225	3800	1	0.0019	31.1	0.078	21.1
79	102	177	2.6	23.8	0.022	0	1	1	225	3800	2	0.0037	31.1	0.118	39.1
80	102	177	2.6	22.6	0.022	0	1	1	225	3800	3	0.0056	26.9	0.157	57.8
81	102	177	2.6	21.6	0.022	0	1	1	225	3800	1	0.0019	31.1	0.078	32.7
82	102	177	2.6	21.6	0.022	0	1	1	225	3800	2	0.0037	28.2	0.118	45.4
83	150	204	4.9	42.9	0.051	0.0013	200	100	270	5270	1	0.0003	29	0.04	70.1
84	150	250	3	36	0.05	0	1	1	230	3800	1	0.0004	74	0.16	66.8
85	150	250	3	36	0.05	0	1	1	230	3800	2	0.0008	74	0.24	87.5
86	150	250	3	36	0.05	0.0025	1	1	230	3800	1	0.0004	74	0.16	68.4
87	150	250	3	36	0.05	0.0025	1	1	230	3800	2	0.0008	74	0.24	72.1
88	150	250	3	36	0.05	0.005	1	1	230	3800	1	0.0004	74	0.16	67.7
89	150	250	3	36	0.05	0.005	1	1	230	3800	2	0.0008	74	0.24	73.6

References

[1] S.M. Abd, I.S. Mhaimeed, B.A. Tayeh, H.M. Najm, S. Qaidi, Investigation of the use of textile carbon yarns as sustainable shear reinforcement in concrete beams, Case Stud. Constr. Mater. 18 (2023), e01765.

[2] O.R. Abuodeh, J.A. Abdalla, R.A. Hawileh, Prediction of shear strength and behavior of RC beams strengthened with externally bonded FRP sheets using machine learning techniques, Compos. Struct. 234 (2020), 111698.

[3] A. Ahmed, S. Elkatatny, A. Ali, M. Mahmoud, A. Abdulraheem, New model for pore pressure prediction while drilling using artificial neural networks, Arab. J. Sci. Eng. 44 (2019) 6079–6088, https://doi.org/10.1007/s13369-018-3574-7.

[4] A. Al-Saidy, A. Al-Harthy, K. Al-Jabri, M. Abdul-Halim, N. Al-Shidi, Structural performance of corroded RC beams repaired with CFRP sheets, Compos. Struct. 92 (2010) 1931–1938.

[5] Y.A. Al-Salloum, H.M. Elsanadedy, S.H. Alsayed, R.A. Iqbal, Experimental and numerical study for the shear strengthening of reinforced concrete beams using textile-reinforced mortar, J. Compos. Constr. 16 (2012) 74–90.

[6] M. Angiolilli, A. Gregori, M. Pathirage, G. Cusatis, Fiber Reinforced Cementitious Matrix (FRCM) for strengthening historical stone masonry structures: experiments and computations, Eng. Struct. 224 (2020), 111102.

[7] A.T. Anvari, S. Babanajad, A.H. Gandomi, Data-Driven prediction models for total shear strength of reinforced concrete beams with fiber reinforced polymers using an evolutionary machine learning approach, Eng. Struct. 276 (2023), 115292.

[8] M.K. Askar, A.F. Hassan, Y.S. Al-Kamaki, Flexural and shear strengthening of reinforced concrete beams using FRP composites: a state of the art, Case Stud. Constr. Mater. (2022), e01189.

[9] R. Azam, K. Soudki, FRCM strengthening of shear-critical RC beams, J. Compos. Constr. 18 (2014), 04014012.

[10] M.S. Barkhordari, D.-C. Feng, M. Tehranizadeh, Efficiency of hybrid algorithms for estimating the shear strength of deep reinforced concrete beams. Periodica Polytechnica, Period. Polytech. Civ. Eng. 66 (2022) 398–410.

[11] C.E. Chalioris, C.P. Papadopoulos, C.N. Pourzitidis, D. Fotis, K.K. Sideris, Application of a reinforced self-compacting concrete jacket in damaged reinforced concrete beams under monotonic and repeated loading, J. Eng. (2013) 2013.

[12] S. Chatterjee, S. Sarkar, S. Hore, N. Dey, A.S. Ashour, V.E. Balas, Particle swarm optimization trained neural network for structural failure prediction of multistoried RC buildings, Neural Comput. Appl. 28 (2017) 2005–2016.

[13] J.-X. Chen, X.-Y. Zhao, A general integrated machine learning pipeline: Its concept, main steps and application in shear strength prediction of RC beams strengthened with FRCM, Eng. Struct. 281 (2023), 115749.

[14] X. Chen, J. Fu, J. Yao, J. Gan, Prediction of shear strength for squat RC walls using a hybrid ANN–PSO model, Eng. Comput. 34 (2018) 367–383.

[15] T. D'Antino, F. Focacci, L.H. Sneed, C. Pellegrino, Shear strength model for RC beams with U-wrapped FRCM composites, J. Compos. Constr. 24 (2020), 04019057.

[16] R. Eberhart, J. Kennedy, A new optimizer using particle swarm theory. held in Nagoya, Jpn., (IEEE) (1995) 39–43.

[17] T. El Maaddawy, K. Soudki, Carbon-fiber-reinforced polymer repair to extend service life of corroded reinforced concrete beams, J. Compos. Constr. 9 (2005) 187–194.

[18] M. Elghazy, El Refai, A. Ebead, U, A. Nanni, Post-repair flexural performance of corrosion-damaged beams rehabilitated with fabric-reinforced cementitious matrix (FRCM), Constr. Build. Mater. 166 (2018) 732–744.

[19] C. Escrig, L. Gil, E. Bernat-Maso, Experimental comparison of reinforced concrete beams strengthened against bending with different types of cementitious-matrix composite materials, Constr. Build. Mater. 137 (2017) 317–329.

[20] C. Escrig, L. Gil, E. Bernat-Maso, F. Puigvert, Experimental and analytical study of reinforced concrete beams shear strengthened with different types of textile-reinforced mortar, Constr. Build. Mater. 83 (2015) 248–260.

[21] F. Faleschini, J. Gonzalez-Libreros, M.A. Zanini, L. Hofer, L. Sneed, C. Pellegrino, Repair of severely-damaged RC exterior beam-column joints with FRP and FRCM composites, Compos. Struct. 207 (2019) 352–363.

[22] A. Ghoniem, Deep learning shear capacity prediction of fibrous recycled aggregate concrete beams strengthened by side carbon fiber-reinforced polymer sheets, Compos. Struct. 300 (2022), 116137.

[23] E.M. Golafshani, A. Ashour, A feasibility study of BBP for predicting shear capacity of FRP reinforced concrete beams without stirrups, Adv. Eng. Softw. 97 (2016) 29–39.

[24] J.H. Gonzalez-Libreros, C. Sabau, L.H. Sneed, C. Pellegrino, G. Sas, State of research on shear strengthening of RC beams with FRCM composites, Constr. Build. Mater. 149 (2017) 444–458.

[25] J.H. Gonzalez-Libreros, L. Sneed, T. D'Antino, C. Pellegrino, Behavior of RC beams strengthened in shear with FRP and FRCM composites, Eng. Struct. 150 (2017) 830–842.
[26] N.F. Grace, G. Sayed, A. Soliman, K. Saleh, Strengthening reinforced concrete beams using fiber reinforced polymer (FRP) laminates, Acids Struct. J. -Am. Concr. Inst. 96 (1999) 865–874.
[27] J. Huang, M. Zhou, J. Zhang, J. Ren, N.I. Vatin, M.M.S. Sabri, The use of ga and pso in evaluating the shear strength of steel fiber reinforced concrete beams, KSCE J. Civ. Eng. 26 (2022) 3918–3931.
[28] S. Iqbal, A. Ali, K. Holschemacher, T.A. Bier, A.A. Shah, Strengthening of RC beams using steel fiber reinforced high strength lightweight self-compacting concrete (SHLSCC) and their strength predictions, Mater. Des. 100 (2016) 37–46.
[29] A. Kaveh, H.R. Bondarabady, Wavefront reduction using graphs, neural networks and genetic algorithm, Int. J. Numer. Methods Eng. 60 (2004) 1803–1815.
[30] A. Kaveh, Y. Gholipour, H. Rahami, Optimal design of transmission towers using genetic algorithm and neural networks, Int. J. Space Struct. 23 (2008) 1–19.
[31] A. Kaveh, H. Servati, Design of double layer grids using backpropagation neural networks, Comput. Struct. 79 (2001) 1561–1568.
[32] G. Loreto, S. Babaeidarabad, L. Leardini, A. Nanni, RC beams shear-strengthened with fabric-reinforced-cementitious-matrix (FRCM) composite, Int. J. Adv. Struct. Eng. (IJASE) 7 (2015) 341–352.
[33] H.-B. Ly, T.-T. Le, H.-L.T. Vu, V.Q. Tran, L.M. Le, B.T. Pham, Computational hybrid machine learning based prediction of shear capacity for steel fiber reinforced concrete beams, Sustainability 12 (2020) 2709.
[34] S.H. Mai, V.-L. Tran, D.-D. Nguyen, V.T. Nguyen, D.-K. Thai, Patch loading resistance prediction of steel plate girders using a deep artificial neural network and an interior-point algorith, Steel Compos. Struct. 45 (2022) 159.
[35] M.H. Makhlouf, M. Mansour, Efficiency of innovative strengthening techniques and anchorage systems using different materials on flexure performance of RC beams, Case Stud. Constr. Mater. 18 (2023), e01733.
[36] A. Marani, M.L. Nehdi, Predicting shear strength of FRP-reinforced concrete beams using novel synthetic data driven deep learning, Eng. Struct. 257 (2022), 114083.
[37] H. Naderpour, P. Parsa, M. Mirrashid, Innovative approach for moment capacity estimation of spirally reinforced concrete columns using swarm intelligence–based algorithms and neural network. Practice Periodical on Structural Design and Construction 26 (2021), 04021043.
[38] B. Nanda, D. Maity, D.K. Maiti, Damage assessment from curvature mode shape using unified particle swarm optimization, Struct. Eng. Mech. 52 (2014) 307–322.
[39] M. Naser, S. Thai, H.-T. Thai, Evaluating structural response of concrete-filled steel tubular columns through machine learning, J. Build. Eng. 34 (2021), 101888, https://doi.org/10.1016/j.jobe.2020.101888.
[40] D.-D. Nguyen, V.-L. Tran, D.-H. Ha, V.-Q. Nguyen, T.-H. Lee, A machine learning-based formulation for predicting shear capacity of squat flanged RC walls, Elsevier, 2021, pp. 1734–1747.
[41] H. Nguyen, H. Moayedi, L.K. Foong, H.A.H. Al Najjar, W.A.W. Jusoh, A.S.A. Rashid, J. Jamali, Optimizing ANN models with PSO for predicting short building seismic response, Eng. Comput. 36 (2020) 823–837.
[42] T.-H. Nguyen, N.-L. Tran, D.-D. Nguyen, Prediction of AXial Compression Capacity of Cold-Formed steel oval hollow section columns using ANN and ANFIS models, Int. J. Steel Struct. (2021) 1–26, https://doi.org/10.1007/s13296-021-00557-z.
[43] T.-H. Nguyen, N.-L. Tran, D.-D. Nguyen, Prediction of critical buckling load of web tapered I-Section steel columns using artificial neural networks, Int. J. Steel Struct. (2021) 1–23.
[44] V.-Q. Nguyen, V.-L. Tran, D.-D. Nguyen, S. Sadiq, D. Park, Novel hybrid MFO-XGBoost model for predicting the racking ratio of the rectangular tunnels subjected to seismic loading, Transp. Geotech. 37 (2022), 100878.
[45] I.M. Nikbin, S. Rahimi, H. Allahyari, A new empirical formula for prediction of fracture energy of concrete based on the artificial neural network, Eng. Fract. Mech. 186 (2017) 466–482, https://doi.org/10.1016/j.engfracmech.2017.11.010.
[46] M. Orouji, E. Najaf, Effect of GFRP rebars and polypropylene fibers on flexural strength in high-performance concrete beams with glass powder and microsilica, Case Stud. Constr. Mater. 18 (2023), e01769.
[47] V.M. Patel, H.B. Mehta, Thermal performance prediction models for a pulsating heat pipe using Artificial Neural Network (ANN) and Regression/Correlation, Anal. (RCA). Sādhanā 43 (2018) 1–16, https://doi.org/10.1007/s12046-018-0954-3.
[48] S.B. Patil, N. Subbareddy, Neural network based system for script identification in Indian documents, Sadhana 27 (2002) 83–97, https://doi.org/10.1007/BF02703314.
[49] R. Perera, A. Arteaga, A. De Diego, Artificial intelligence techniques for prediction of the capacity of RC beams strengthened in shear with external FRP reinforcement, Compos. Struct. 92 (2010) 1169–1175.
[50] J. Rahman, K.S. Ahmed, N.I. Khan, K. Islam, S. Mangalathu, Data-driven shear strength prediction of steel fiber reinforced concrete beams using machine learning approach, Eng. Struct. 233 (2021), 111743.
[51] S.M. Raoof, L.N. Koutas, D.A. Bournas, Textile-reinforced mortar (TRM) versus fibre-reinforced polymers (FRP) in flexural strengthening of RC beams, Constr. Build. Mater. 151 (2017) 279–291.
[52] M. Rönnholm, K. Arve, K. Eränen, F. Klingstedt, T. Salmi, H. Saxén, ANN modeling applied to NO X reduction with octane. A nn future in personal vehicles. Adaptive and Natural Computing Algorithms, Springer, 2005, pp. 100–103, https://doi.org/10.1007/3-211-27389-1_24.
[53] S.S. Selvan, P.S. Pandian, A. Subathira, S. Saravanan, Comparison of response surface methodology (RSM) and artificial neural network (ANN) in optimization of Aegle marmelos oil extraction for biodiesel production, Arab. J. Sci. Eng. 43 (2018) 6119–6131, https://doi.org/10.1007/s13369-018-3272-5.
[54] T. Sevil, M. Baran, T. Bilir, E. Canbay, Use of steel fiber reinforced mortar for seismic strengthening, Constr. Build. Mater. 25 (2011) 892–899.
[55] S.P. Shah, A.E. Naaman, Mechanical properties of glass and steel fiber reinforced mortar, In 1 (1976) 50–53.
[56] A. Siddika, M.A. Al Mamun, R. Alyousef, Y.M. Amran, Strengthening of reinforced concrete beams by using fiber-reinforced polymer composites: a review, J. Build. Eng. 25 (2019), 100798.
[57] K. Sideris, P. Manita, A. Papageorgiou, E. Chaniotakis, Mech. Charact. High. Perform. Fibre Reinf. Concr. Elev. Temp. (2003) 973–988.
[58] L.H. Sneed, S. Verre, C. Carloni, L. Ombres, Flexural behavior of RC beams strengthened with steel-FRCM composite, Eng. Struct. 127 (2016) 686–699.
[59] R. Solhmirzaei, H. Salehi, V. Kodur, M. Naser, Machine learning framework for predicting failure mode and shear capacity of ultra high performance concrete beams, Eng. Struct. 224 (2020), 111221.
[60] B. Tahmouresi, K. Momeninejad, E. Mohseni, Flexural response of FRP-strengthened lightweight RC beams: hybrid bond efficiency of L-shape ribbed bars and NSM technique, Arch. Civ. Mech. Eng. 22 (2022) 95.
[61] B. Tahmouresi, P. Nemati, M.A. Asadi, A. Saradar, M.M. Moein, Mechanical strength and microstructure of engineered cementitious composites: a new configuration for direct tensile strength, experimental and numerical analysis, Constr. Build. Mater. 269 (2021), 121361.
[62] N.-L. Tran, D.-D. Nguyen, T.-H. Nguyen, Prediction of speed limit of cars moving on corroded steel girder bridges using artificial neural networks, Sādhanā 47 (2022) 1–14.
[63] Tran, N.-L., Nguyen, T.-H., Phan, V.-T., Nguyen, D.-D. A Machine Learning-Based Model for Predicting Atmospheric Corrosion Rate of Carbon Steel. Advances in Materials Science and Engineering *2021*.
[64] V.-L. Tran, S.-E. Kim, Efficiency of three advanced data-driven models for predicting axial compression capacity of CFDST columns, Thin-Walled Struct. 152 (2020), 106744, https://doi.org/10.1016/j.tws.2020.106744.
[65] V.-L. Tran, D.-D. Nguyen, Novel hybrid WOA-GBM model for patch loading resistance prediction of longitudinally stiffened steel plate girders, Thin-Walled Struct. 177 (2022), 109424.
[66] V.-L. Tran, D.-K. Thai, S.-E. Kim, Application of ANN in predicting ACC of SCFST column, Compos. Struct. 228 (2019), 111332, https://doi.org/10.1016/j.compstruct.2019.111332.
[67] T.C. Triantafillou, C.G. Papanicolaou, Shear strengthening of reinforced concrete members with textile reinforced mortar (TRM) jackets, Mater. Struct. 39 (2006) 93–103.

[68] G.G. Triantafyllou, T.C. Rousakis, A.I. Karabinis, Corroded RC beams patch repaired and strengthened in flexure with fiber-reinforced polymer laminates, Compos. Part B: Eng. 112 (2017) 125–136.

[69] B. Vakhshouri, S. Nejadi, Prediction of compressive strength of self-compacting concrete by ANFIS models, Neurocomputing 280 (2018) 13–22, https://doi.org/10.1016/j.neucom.2017.09.099.

[70] T.G. Wakjira, A. Al-Hamrani, U. Ebead, W. Alnahhal, Shear capacity prediction of FRP-RC beams using single and ensenble ExPlainable Machine learning models, Compos. Struct. 287 (2022), 115381.

[71] T.G. Wakjira, U. Ebead, Hybrid NSE/EB technique for shear strengthening of reinforced concrete beams using FRCM: Experimental study, Constr. Build. Mater. 164 (2018) 164–177.

[72] T.G. Wakjira, U. Ebead, M.S. Alam, Machine learning-based shear capacity prediction and reliability analysis of shear-critical RC beams strengthened with inorganic composites, Case Stud. Constr. Mater. 16 (2022), e01008.

[73] Yang, H., Akiyama, T., and Sasaki, T., 1992. A neural network approach to the identification of real time origin-destination flows from traffic counts.

[74] S. Zhang, Y. Ke, S. Smith, H. Zhu, Z. Wang, Effect of FRP U-jackets on the behaviour of RC beams strengthened in flexure with NSM CFRP strips, Compos. Struct. 256 (2021), 113095.

[75] K. Zorlu, C. Gokceoglu, F. Ocakoglu, H. Nefeslioglu, S. Acikalin, Prediction of uniaxial compressive strength of sandstones using petrography-based models, Eng. Geol. 96 (2008) 141–158, https://doi.org/10.1016/j.enggeo.2007.10.009.